Journal of Materials Chemistry A

ROYAL SOCIETY OF CHEMISTRY

PAPER

View Article Online
View Journal | View Issue

Cite this: J. Mater. Chem. A, 2025, 13, 8466

Enhancing redox stability of lithium–oxygen batteries *via* introducing an oxygen pre-coordinated vanadyl phthalocyanine catalyst†

Boran Kim,‡[a] Hyunji Kweon,‡[bcd] Yeji Lim,‡[a] Hyunyoung Park,[bcd] Jongsoon Kim *[bcd] and Won-Hee Ryu *[a]

Received 4th October 2024
Accepted 6th February 2025

DOI: 10.1039/d4ta07071b

rsc.li/materials-a

Since various metal phthalocyanines (MPcs) possesses the properties of transferring electrons and spontaneously binding with oxygen species, their application as catalysts in Li–O_2 batteries (LOBs) can stabilize the highly active superoxide radical (O^{2-}) to suppress side reactions, leading to enhanced electrochemical performance. MPcs have usually considered common binding behavior directly with empty metal center. However, no attempt has been made to employ MPcs with pre-coordination of the oxygen group on the metal center, which can result in unexpected catalytic behavior. In this work, we demonstrate that a novel oxygen-pre-coordinated MPc catalyst, vanadyl phthalocyanine (VOPc), can facilitate the formation and decomposition of Li-containing discharge products, such as Li_xO_2, during charging/discharging in LOBs. This results in enhanced electrochemical performance, including decreased polarization and stable cycling-performance. Moreover, redox mediation and reaction pathways in the oxygen-pre-coordinated VOPc-applied LOB are confirmed through combined studies using first-principles calculations and various experiments, clearly supporting that the effective catalytic effect of oxygen-pre-coordinated VOPc affords the outstanding electrochemical properties of the LOB.

1. Introduction

Li–O_2 batteries (LOBs), which have a high energy density (>3500 W h kg^{-1}), have recently been highlighted as a next-generation energy storage system that uses lightweight elements such as oxygen and Li.[1–5] It was reported that solid-state Li_xO_2 is reversibly formed/decomposed on the surface of the cathode during charging/discharging in LOBs through an oxygen reduction reaction (ORR) and oxygen evolution reaction (OER) ($xLi^+ + O_2 + xe^- \leftrightarrow Li_xO_2$, $x = 1$ or 2).[6,7] However, the insulating properties of solid-state Li_xO_2 formed after discharging can negatively influence OER kinetics and efficiency during charge, which can result in poor electrochemical performance of LOBs, such as large overpotential and poor cycling-performance.

To solve the problems of LOBs, application of an appropriate redox mediator (RM) by directly dissolving it in liquid electrolytes is considered an effective way to enable smoother decomposition of discharge products (Li_xO_2) during charging and lower the overpotential through efficient liquid–solid contact. In addition, it is known that most RMs participate in electrochemical reactions through direct reduction or oxidation during discharging/charging, and they can diffuse into the discharge products to chemically donate or withdraw electrons.[8–11] Typically, one of the most commonly used redox mediators is metal phthalocyanine (MPc). In fact, MPc is an aromatic macrocyclic organic compound with various transition metals present at the center of the structure. The metal-N_4 center, supported in microporous carbon, exhibited outstanding OER and ORR activities, similar to those observed in Pt-based catalysts, and the possibility of MPc as an outstanding catalyst in actual fuel cells has already been verified.[12–15] In addition, owing to the transition metal atom in the center of its structure, MPc is known to have high solubility in organic solvents with auto-oxygen binding properties even in a low O_2 environment.[16–21]

Therefore, we used metal phthalocyanine as an electrolyte catalyst and confirmed that MPc improves the performance of Li–O_2 batteries. According to our previous research, (1) MPcs successfully stabilized highly active superoxide ions (O_2^-) by binding to them in LOBs, thereby suppressing side reactions, such as electrolyte decomposition. (2) Furthermore, it was

[a]Department of Chemical and Biological Engineering, Sookmyung Women's University, 100 Cheongpa-ro 47-gil, Yongsan-gu, Seoul, 04310, Republic of Korea. E-mail: whryu@sookmyung.ac.kr

[b]Department of Energy Science, Sungkyunkwan University, 2066 Seobu-ro, Jangan-gu, Suwon, 16419, Republic of Korea. E-mail: jongsoonkim@skku.edu

[c]SKKU Institute of Energy Science and Technology (SIEST), Sungkyunkwan University, 2066 Seobu-ro, Jangan-gu, Suwon, 16419, Republic of Korea

[d]KIST-SKKU Carbon-Neutral Research Center, Sungkyunkwan University, Suwon, 16419, Republic of Korea

† Electronic supplementary information (ESI) available. See DOI: https://doi.org/10.1039/d4ta07071b

‡ These authors contributed equally to this work.

confirmed that different MPcs, such as CoPc, CuPc, MnPc, and ZnPc, exhibit distinct binding properties and active sites with superoxide ions depending on their metal type. In addition, it was discovered that there are different stabilization tendencies depending on the metal type in the MPc molecule. Until recently, various related studies on MPcs, including ours, have considered the catalytic effects of binding directly to empty metal centers. Nevertheless, there have been no attempts to use pre-coordinated MPc with an oxygen group on the metal center, which can result in unexpected catalytic effects for the enhanced electrochemical performance of LOBs.

Herein, we investigated whether vanadyl phthalocyanine (VOPc), a novel oxygen-pre-coordinated MPc catalyst, delivered outstanding catalytic effects to enhance the electrochemical performance of LOBs, such as decreased polarization and stable cycle performance, by facilitating the formation and decomposition reaction of Li-containing discharge products (Li_xO_2) during charging/discharging (Fig. 1). Through UV-visible spectra, it was verified that oxygen-pre-coordinated VOPc can effectively bind oxygen ions in the pre-oxygenated central metal in the MPc-type molecule. The outstanding catalytic effect of oxygen-pre-coordinated VOPc in LOBs was also confirmed through first-principles calculations, showing successful redox mediation and enhanced OER kinetics by easier decomposition of solid-state Li_xO_2 during charging.

2. Experimental

2.1 Materials

High purity multi-walled carbon nanotubes (MWCNTs) were donated by SouthWest Nanotechnologies. Vanadyl phthalocyanine (VOPc), tetraethylene glycol dimethyl ether (TEGDME, 99%), bis(trifluoromethane)sulfonimide lithium salt (LiTFSI, 99.95%), poly(vinylidene fluoride) (PVdF, Mw ≈ 180 000), *N*-methyl-2-pyrrolidone (NMP, anhydrous, 99.5%), and potassium dioxide (KO_2) were purchased from Sigma–Aldrich (Korea). We removed residual moisture from TEGDME by dipping freshly activated molecular sieves (4 Å) into the solvent for two weeks.

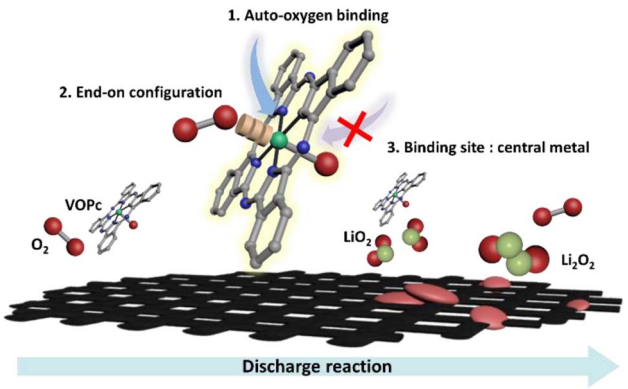

Fig. 1 Catalytic reaction properties of oxygen-pre-coordinated vanadyl phthalocyanine (VOPc) and schematic of reaction intermediates and mechanisms in Li–O_2 cells.

2.2 Material characterization

The crystalline properties were investigated using X-ray diffraction (XRD). Raman, Fourier transform infrared (FT-IR), and X-ray photoelectron spectroscopy (XPS, K-alpha, Thermo U.K.) were performed to characterize and analyse the electrode surface after discharging/charging. Additionally, using field-emission scanning electron microscopy (FE-SEM), we observed MWCNT-loaded Ni-foam electrodes. The time-course ultraviolet-visible spectra (UV-vis, UV-2550, Shimadzu) were used to investigate the oxygen binding effect of vanadyl phthalocyanine.

2.3 Preparation of Li–O_2 cells

The oxygen electrode was prepared using multi-walled carbon nanotubes (MWCNTs, 90 wt%) and PVdF (10 wt%) dissolved in NMP. The slurry was pasted onto a ϕ 12 mm Ni-foam and dried overnight at 80 °C under vacuum conditions. For the oxygen-pre-coordinated VOPc-containing electrolyte, vanadyl phthalocyanine (0.1 g) and LiTFSI (1 M) were diluted in TEGDME (0.5 mL) and stirred for 24 h in an Ar-filled glovebox to saturate the oxygen-pre-coordinated VOPc-containing solution. In the cyclic voltammetry (CV) cycling test, a coin cell including several holes was used. All the cells were assembled in a glove box filled with pure Ar. After assembly, the cells were purged with O_2 (99.999%) before the electrochemical test.

2.4 Calculational details

For the MPc-type molecules, the geometry was optimized and the energy was evaluated using the Gaussian 16 software package. For all the calculations, spin-unrestricted density functional theory (DFT) was performed based on the Becke–Lee–Yang–Parr (B3LYP) hybrid exchange–correlation functional and the triple-zeta valence polarization (TZVP) basis set.[22–28] The calculated molecular structure of MPc was visualized using Avogadro software.[29] The TEGDME solvation was considered by applying a dielectric constant of 7.9, as used in previous studies.[22,23]

2.5 Electrochemical characterization

The catalytic activity of the oxygen-pre-coordinated VOPc-containing Li–O_2 cells was analyzed using cyclic voltammetry (Biologic VSP potentiostat with an impedance function) in the range of 2.0–4.5 V at 5 mV s^{-1}. The charging/discharging tests were performed using a potentiostat/galvanostat (WonATech, Co., Ltd, WBCS3000, Korea) at 100 mA g^{-1} in the range of 2.3–4.5 V *vs.* Li/Li^+. For the cycling tests, a potentiostat/galvanostat (WonATech, Co., Ltd, WBCS3000L, Korea) was used at 100 mA g^{-1} with a limited capacity of 1000 mA h g^{-1} in the same voltage range as the charging/discharging tests. Before the electrochemical tests, the cells were purged with O_2 gas, and the tests were performed at room temperature.

3. Results and discussion

3.1 Electrochemical properties of oxygen-pre-coordinated VOPc-applied LOB cells

To confirm the catalytic activities of oxygen-pre-coordinated VOPc in LOBs, we compared the cyclic voltammetry (CV) results of the pristine and the oxygen-pre-coordinated VOPc-based electrolytes (Fig. 2a). In the case of the cathodic reaction, the ORR onset potential was increased by applying the oxygen-pre-coordinated VOPc (≈2.80 V) than the pristine cell (≈2.72 V), and the ORR current in the oxygen-pre-coordinated VOPc-applied cell tremendously increased than in the pristine cell. Through the reaction process, it was verified that the ORR rate in the oxygen-pre-coordinated VOPc-applied cell that can bind with O_2 and shuttle it to the electrode is faster than that in the pristine cell.[21,30,31] In the case of the anodic reaction, we confirmed that the onset potential of the oxygen-pre-coordinated VOPc-applied cell decreased (≈2.98 V) compared to that of the pristine (≈3.09 V) cell, and the reaction current of the oxygen-pre-coordinated VOPc-applied cell dramatically increased. With these results, the cell overpotential with oxygen-pre-coordinated VOPc was decreased by half that of the pristine cell. The most obvious difference according to the existence of oxygen-pre-coordinated VOPc was the peak formation at the 3.45 V region. This voltage region is where one Li^+ is delithiated from Li_2O_2 to the outer side to form LiO_2 ($Li_2O_2 \rightarrow Li^+ + e^- + LiO_2$); then, two LiO_2 disproportionate to chemically evolve O_2 ($2LiO_2 \rightarrow Li_2O_2 + O_2$).[32,33] As the center metal of MPc can stabilize O^{2-} by binding it, MPc can mediate the charge process and induce a disproportionation reaction than direct oxidation reaction, which can operate at a much higher voltage range.[31,34]

To evaluate the cell performance on the actual operation of LOBs, the discharge–charge curves between the pristine and the oxygen-pre-coordinated VOPc-applied cells were compared

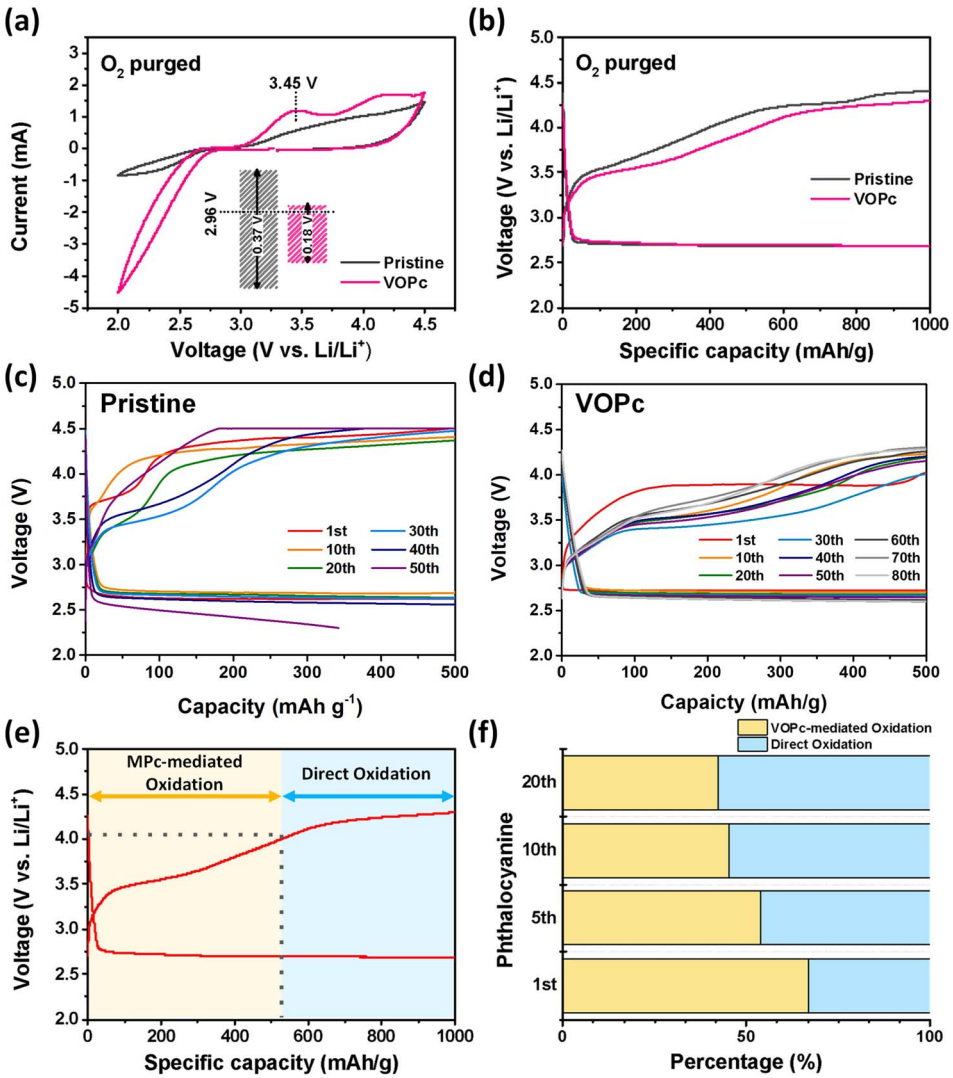

Fig. 2 Electrochemical properties. (a) Cyclic voltammetry (CV) curves obtained for Li–O_2 cells employing VOPc. (b) Discharge–charge curves measured in the 2.3–4.5 V window for Li–O_2 cells fabricated using pristine and VOPc containing electrolytes. (c and d) Cycling performance of the pristine and VOPc-applied Li–O_2 cells in the range of 2.3–4.5 V. (e and f) Ratios of "metal phthalocyanine-mediated oxidation (MPc-mediated oxidation)" and "direct oxidation" during charging of VOPc-containing cells.

(Fig. 2b). During the discharge reaction, all cells showed a plateau at around 2.72 V, which is known as the region on the formation of Li_2O_2.[21,35] In the charge curve, a bump was formed at around 3.45 V in all cells, which indicates the region where oxygen is evolved by the disproportionation reaction.[32,33] In the pristine cell, the operation voltage rapidly increased after the bump formation. However, the operation voltage of the oxygen-pre-coordinated VOPc-applied cell was slowly polarized after the bump formation, and it showed much lower cell overpotential during charging than the pristine cell. To evaluate the lifetime of the oxygen-pre-coordinated VOPc activity and the improvement of the cell cycling life by applying oxygen-pre-coordinated VOPc, the discharge–charge curves in various cycle numbers of pristine and oxygen-pre-coordinated VOPc-applied cells were compared, as shown in Fig. 2c and d. The ORR overpotential of both cells gradually increased as the cycle number increased. However, the OER operation trend showed a distinguishing difference between the pristine and oxygen-pre-coordinated VOPc-applied cells. In the pristine cell, the charge curves in the early cycles showed a typical disproportionation reaction and direct oxidation reaction trend. The bump formation voltage continuously increased, resulting in cell polarization, and most of the reaction occurred above 4.0 V, where the direct oxidation reaction is dominant. Moreover, the reversibility of the cell deteriorated after the 40th cycle. However, in the case of the oxygen-pre-coordinated VOPc-applied cell, the bump formation voltage was relatively well maintained until the 80th cycle. Additionally, the coulombic efficiency of the VOPc-applied cell was evaluated, and it was observed to maintain 100% efficiency up to 80 cycles (Fig. S1†). Through the comparison of electrochemical performances in the pristine and oxygen-pre-coordinated VOPc-applied cells, it was verified that applying oxygen-pre-coordinated VOPc in LOBs can stabilize the O^{2-} and induce the disproportionation reaction reducing the cell overpotential. However, if pre-occupied oxygen exists with the central metal, the access and adsorption of reactants can be inhibited, declining the catalytic effect. Therefore, we compared the electrochemical performances between the oxygen-pre-coordinated VOPc and various types of MPc without pre-coordinated oxygen, such as CuPc and NiPc, to objectively evaluate the activity of oxygen-pre-coordinated VOPc (Fig. S2 and S3†). In the CV curve, all MPc-applied cells showed lower overpotential and higher reactivity than pristine cells in ORR/OER, and distinct O^{2-} peaks were formed at around 3.45 V when MPc was introduced. Moreover, by evaluating the activity between the MPcs, we found that oxygen-pre-coordinated VOPc showed the highest activity in the cathodic reaction, and oxygen-pre-coordinated VOPC and NiPc showed similar activity in the anodic reaction. CuPc showed the lowest activity among them. In the discharge–charge cycle curve, which represents the cell performance under actual cell operation conditions, the activity of each MPc was more clearly evaluated. In the discharge curve, all cells showed a similar operation voltage ($\approx$2.72 V), demonstrating that additional polarization was not required for the reactant absorption on oxygen-pre-coordinated VOPc. In the charge reaction, the disproportionation reaction continued most stably in the oxygen-pre-coordinated VOPc-applied cell, and the polarization rate was also lowest with oxygen-pre-coordinated VOPc. Based on these results, we verified the strong catalytic effect of oxygen-pre-coordinated VOPc and whether there was a blocking effect by pre-occupied oxygen or not.

To quantitatively evaluate the catalytic effect of oxygen-pre-coordinated VOPc to stabilize O^{2-} by mediating the charge reaction, we divided the OER curve into two sections, 'MPc-mediated oxidation' and 'direct oxidation', and compared the fraction of two parts in the charging process (Fig. 2e). As the beginning of the OER is related to LiO_2 formation and Li_2O_2 can be directly decomposed at over 4.0 V, the 4.0 V was set as the standard. The capacity region where the operation voltage was lower than the standard was labeled as 'MPc-mediated oxidation', and the region higher than it was labeled as 'Direct oxidation'.[21,32,34] This standard can be supported by the bumps formed around 3.4 V and 4.0 V in all cells, as illustrated in Fig. 2b, indicating the reaction method change. We compared the MPc-mediated reaction fractions among the pristine cell and oxygen-pre-coordinated VOPc- and other MPc-applied cells (Fig. S4 and S5†). In the pristine cell, the OER activity was 100% caused by direct oxidation because MPc was not included in the electrolyte. When MPc was applied in LOBs, the fractions of MPc-mediated oxidation with NiPc, CuPc and oxygen-pre-coordinated VOPc were $\sim$41.36%, $\sim$44.95%, and $\sim$52.78%, respectively, implying that oxygen-pre-coordinated VOPc induces stronger redox mediation during OER in LOBs than in NiPc and CuPc. In addition, we compared the proportion of the MPc-mediated and direct oxidation reaction in various cycles of oxygen-pre-coordinated VOPc-applied cells and confirmed the maintenance of the oxygen-pre-coordinated VOPc-mediated oxidation reaction (Fig. 2f). In the first cycle, the ratio of oxygen-pre-coordinated VOPc-mediated oxidation was about 70%, which demonstrated that the catalytic effect was effectively exhibited by binding superoxide radical ion (O^{2-}) to oxygen pre-coordinated VOPc during the charge reaction. Moreover, although the ratios decreased in the 5th and 10th cycles as the reaction continued, the superoxide radical ion (O^{2-}) stabilization effect of oxygen-pre-coordinated VOPc was clearly shown and tended to converge to some extent, indicating that the O^{2-} stabilization effect of oxygen-pre-coordinated VOPc was maintained even if the cycle continued.

3.2 Catalytic reaction reversibility by applying oxygen-pre-coordinated VOPc

To evaluate the reaction reversibility and the structural changes during charging/discharging, the *ex situ* analysis of pristine, discharged and charged oxygen electrodes with oxygen-pre-coordinated VOPc was conducted (Fig. 3). The morphology change in the oxygen electrode during the cycling was estimated with the magnified scanning electron microscopy (SEM) images (Fig. 3a–c). For the pristine electrode, the CNT active material was well loaded on the nickel foam, and a film-like discharge product was formed around the active material after discharging (Fig. 3a and b). In the charge electrode image in Fig. 3c, the discharge product was reversibly decomposed, and there was no

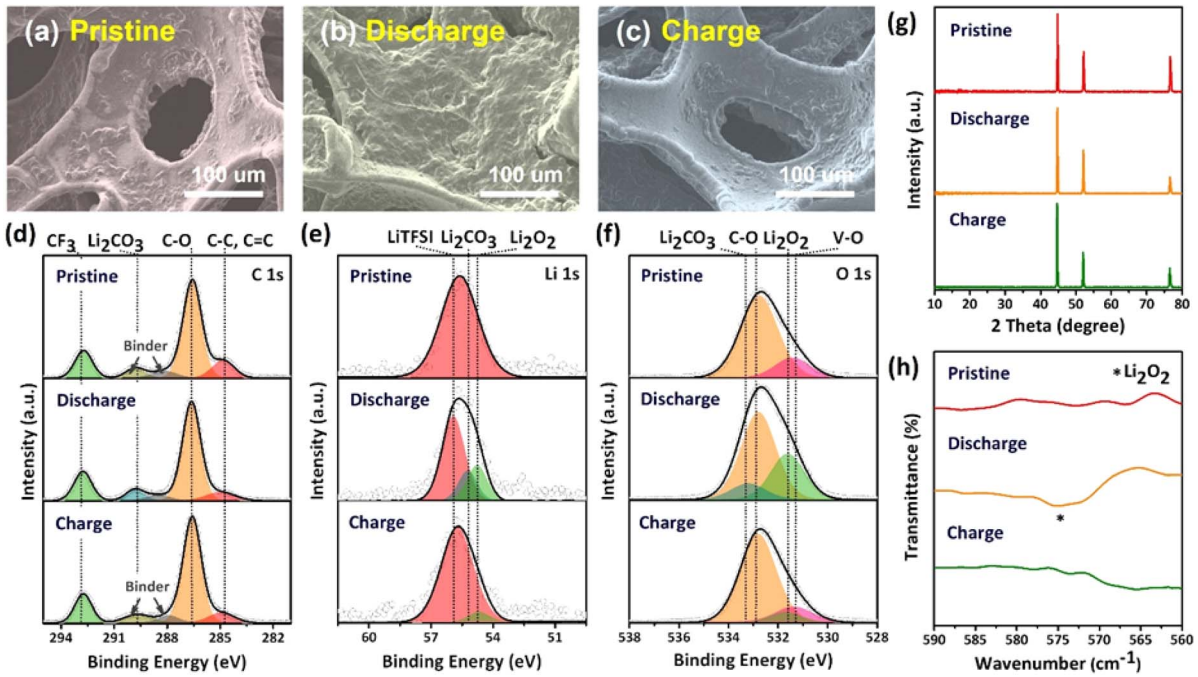

Fig. 3 Morphologies, crystal information and chemical composition of electrode applying VOPc. SEM image of (a) the pristine electrode, (b) discharge electrode and (c) charge electrode. *Ex situ* XPS spectra of the pristine, discharge, and charge electrodes with the VOPc applied electrolyte: (d) C 1s, (e) Li 1s, and (f) O 1s spectra. (g) *Ex situ* XRD patterns and (h) *ex situ* FT-IR patterns of the pristine, discharge, and charge electrodes with the VOPc applied electrolyte.

collapse of the electrode structure. For the comparison of the carbon-based electrode surface involving material changes during the cell operation, the C 1s X-ray photoelectron spectroscopy (XPS) spectra were estimated (Fig. 3d). As oxygen was purged on all three cells, including pristine, O_2 was absorbed on the CNT electrode, and the C–O peak with high intensity appeared at the 286.6 eV position. This peak was slightly increased after discharging, demonstrating that the discharge product (Li_2O_2) chemically reacted with a carbon-based oxygen electrode to form Li_2CO_3 $\left(Li_2O_2 + C + \frac{1}{2}O_2 \rightarrow Li_2CO_3\right)$ or the occurrence of the side reaction with the organic electrolyte.[24,35] Thus, evidence of the formation of Li_2CO_3 was observed through the peak at 289.8 eV, while the coverage of discharge products and byproducts on the discharge electrode led to a decrease in the C–C peak at 284.7 eV. However, during the charge process, the Li_2CO_3 peak disappeared as it electrochemically decomposed ($2Li_2CO_3 \rightarrow 4Li^+ + 2CO_2 + O_2 + 4e^-$).[8] Moreover, significant change was not observed in the C–C peak as the evolved O_2 bonded with the neighboring carbon electrode. The CF_3 peak with the same intensity appeared on all three electrodes, which represents LiTFSI salts remaining on the electrode surface, and was detected at 292.8 eV. In Li 1s spectra, the LiTFSI peak (55.6 eV), which indicates the residual salt in the electrolyte, was observed in all three electrodes (Fig. 3e). After discharging, the discharge product (Li_2O_2) and byproduct ($LiCO_3$) peak were presented at 54.8 eV and 55.2 eV, respectively. In the charge electrode, the byproduct was entirely decomposed, and the discharge product peak intensity decreased. The reaction reversibility of the LOB cell with oxygen-pre-coordinated VOPc can also be confirmed with the O 1s spectra (Fig. 3f). Similar to the C 1s spectra analysis, the C–O peak (532.9 eV) slightly increased after discharging and was maintained after recharge. The Li_2O_2 peak (531.6 eV) was observed on the discharge electrode surface, but its intensity decreased on the charge electrode. The Li_2CO_3 peak (533.3 eV) was formed and disappeared after discharging and charging, respectively. Moreover, the V–O peak was detected at 531.3 eV on the O 1s spectra, which is a peak for pre-coordinated oxygen binding to the oxygen-pre-coordinated VOPc central metal remaining on the electrode surface. As the discharge electrode was covered with the discharge products and the byproduct, the V–O peak did not appear predominantly on it. However, on the charge electrode, a clear V–O peak reappeared with a similar intensity to the pristine one. Through these results, we confirmed that the oxygen attached to oxygen-pre-coordinated VOPc was well maintained during cycling, and oxygen-pre-coordinated VOPc only mediated the LOB cell reaction without the structural change.

To identify the crystallinity of the discharge product, the X-ray diffraction (XRD) patterns of pristine, discharge and charge electrodes were obtained (Fig. 3g). In the XRD pattern on all the three electrodes, only the CNT lattice peak was detected, and the Li_2O_2 lattice peak was not observed. Based on this result, we conclude that the Li_2O_2 was formed in an amorphous phase. This result is consistent with the film-like morphology of the discharge electrode discussed in the SEM image. Formation of amorphous phase Li_2O_2 is a common result when the LOB

cell is operated with a low donor number solvent, such as tetraethylene glycol dimethyl ether (TEGDME).[33,36] The reaction reversibility of LOB cells was also demonstrated by the Fourier Transform Infrared Spectroscopy (FT-IR) pattern (Fig. 3h). The Li_2O_2 peak (574.7 cm^{-1}) was generated after discharging and disappeared after charging.

3.3 Specific reaction mechanism of oxygen-pre-coordinated VOPc

We performed real-time ultraviolet-visible (UV-vis) spectrophotometry analysis to confirm the auto-oxygen binding properties of oxygen-pre-coordinated VOPc after injecting KO_2 solution in the electrolyte and monitored the changes in absorbance at different times after oxygen binding (Fig. 4a). Additionally, we found out why the performance of oxygen-pre-coordinated VOPc can be well expressed even in pre-coordinated with the oxygen group through UV-vis analysis data. Research has already been conducted on the binding properties of phthalocyanines with an empty metal centers (CoPc, CuPc, MnPc, and ZnPc) through the US-vis spectra of four MPcs (Fig. S6†).[21] It was confirmed that the binding properties of various metal phthalocyanines vary according to the d-orbital occupation of the central metal, and 'side-on', 'end-on', and 'side group' binding configurations are formed. In the case of oxygen-pre-coordinated VOPc to which oxygen is already bonded, it may be observed that the intensity of the peak increased compared to pristine immediately after KO_2 was injected. However, because the d-orbital of vanadium is unoccupied, and only the intensity of the peak has changed without peak shifting, it can be observed that superoxide ions bound to the central metal of

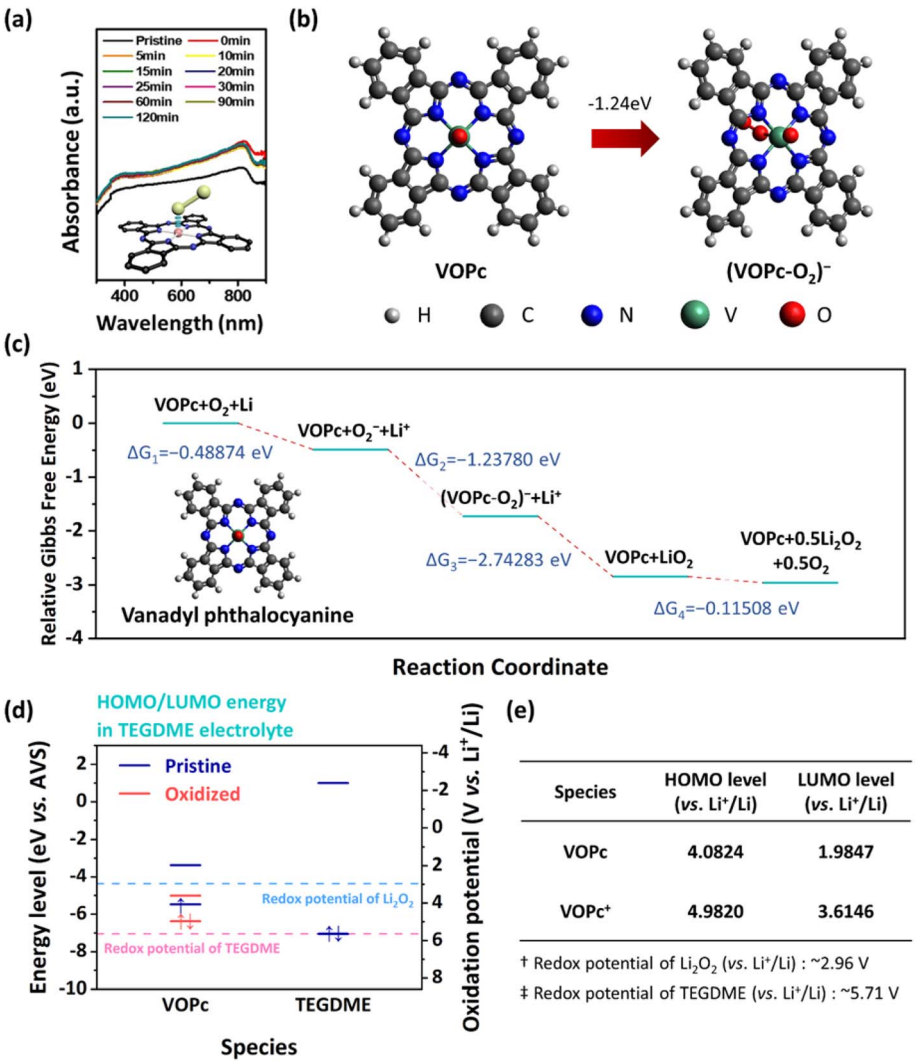

Fig. 4 (a) Ultraviolet-visible (UV–vis) spectra of vanadyl phthalocyanine (VOPc) at different times after superoxide injection using KO_2 solution. Wavelength range of 350–850 nm was applied to detect the state of VOPc central metal atoms. If states of central metals are altered, some peaks would shift or change in that range. (b) Molecular structure of pristine VOPc and $(VOPc\text{-}O_2)^-$. (c) Relative Gibbs free-energy diagrams generated for cell-reaction intermediates in the oxygen-pre-coordinated VOPc-containing Li–O_2 cell. (d) DFT-based highest occupied molecular orbital (HOMO) and lowest unoccupied molecular orbital (LUMO) energies of pristine VOPc and oxidized $VOPc^+$ in TEGDME. (e) Predicted molecular orbital energies of pristine VOPc and oxidized $VOPc^+$ adjusted for oxidation potential (*vs.* Li^+/Li).

oxygen-pre-coordinated VOPc and form an 'end-on' configuration.

In addition, similar results were obtained through first-principles calculations. As shown in Fig. 4b, the oxygen-pre-coordinated VOPc molecule is bonded with the oxygen group in the pristine state. Subsequently, calculations were carried out by assuming that the superoxide ion binds to the central metal site of oxygen-pre-coordinated VOPc. By comparing the Gibbs free energies of pristine structure and superoxide-bonded structure, we confirmed that the oxygen-pre-coordinated VOPc molecule prefers to form an 'end-on' configuration, lowering the total free energy by −1.24 eV. Furthermore, we predicted the detailed reaction mechanism of oxygen-pre-coordinated VOPc in the LOB cell by analyzing the free energies of each reaction intermediate and product (Fig. 4c). During the ORR process, the highly reactive superoxide is effectively stabilized by the oxygen-pre-coordinated VOPc molecule, which captures it in the form of $(VOPc\text{-}O_2)^-$. Subsequently, the $(VOPc\text{-}O_2)^-$ complexes react with neighboring Li^+ to form Li_xO_2 products. Throughout a series of reactions, the total free energy continuously decreased, indicating that spontaneous catalytic reactions occurred. Moreover, we demonstrated the outstanding catalytic effect of VOPc as the effective RM for LOBs using first-principles calculation. As shown in Fig. 4d and e, we compared the theoretical highest occupied molecular orbital (HOMO) and the lowest unoccupied molecular orbital (LUMO) energy levels of pristine VOPc and oxidized $VOPc^+$ using the TEGDME dielectric constant (7.9) considering the TEGDME-based electrolyte. The blue and red bars indicate the relative values of pristine VOPc and oxidized $VOPc^+$ *vs.* absolute vacuum scale (AVS), respectively. It was reported that the AVS is −4.44 V *vs.* standard hydrogen electrode (SHE). Thus, the 0 V *vs.* Li^+/Li corresponds to −1.39 eV *vs.* AVS, and the formation redox potential of Li_2O_2 is approximately −4.35 eV (*vs.* AVS). As the decomposition of Li_2O_2 occurs at approximately 2.96 V (*vs.* Li^+/Li; shown by the dotted blue line) and the redox potential of the pristine VOPc is higher than 2.96 V, Li_2O_2 can decompose in the electrolyte containing TEGDME and oxygen-pre-coordinated VOPc. Moreover, it was verified that the HOMO energies of the oxidized $VOPc^+$ were higher than those of the TEGDME (~5.71 V *vs.* Li^+/Li; shown by the dotted red line), indicating that there is no decomposition of TEGDME during charging. These calculation results showed that oxygen-pre-coordinated VOPc can be used as an outstanding and effective RM catalyst with the stable redox operation of LOBs.

We monitored the structural changes in VOPc added to the Li–O_2 system as the voltage decreased from 3.3 V to 2.0 V (discharge) and then increased from 2.0 V to 4.0 V (charge), confirming the reaction facilitation mechanism of VOPc based on these results and previous experiments (Fig. S7 and S8†). First, according to the UV-vis results, an intensity peak related to the vanadium metal was observed around 300 nm at an initial voltage of 3.3 V. During the oxygen reduction reaction (ORR), as the voltage decreased to 2.0 V, oxygen was reduced to form reactive oxygen radicals (O_2^-), which were stabilized by VOPc through the formation of VOPc-O_2 complexes, preventing undesirable side reactions. These complexes subsequently reacted with Li^+ to form lithium oxides (*e.g.*, LiO_2 and Li_2O_2), and VOPc was regenerated to its original state in the process. Simultaneously, the UV-vis results revealed structural changes indicated by a decrease in the intensity of the peak. During the oxygen evolution reaction (OER), as the voltage increased from 2.0 V to 4.0 V, VOPc was oxidized to $VOPc^+$ ($2VOPc \rightarrow 2VOPc^+ + 2e^-$). $VOPc^+$ reacted with Li_2O_2 ($2VOPc^+ + Li_2O_2 \rightarrow 2VOPc + 2Li^+ + O_2$), or in a direct OER pathway, Li_2O_2 decomposed ($Li_2O_2 \rightarrow 2Li^+ + O_2^- + e^-$). The resulting oxygen radicals were stabilized by VOPc-O_2 complexes. In this process, the intensity peak related to the vanadium central metal reappeared reversibly, as confirmed by the UV-vis results.

4. Conclusions

In summary, the oxygen binding effect and catalytic effect of oxygen-pre-coordinated VOPc, in which oxygen has been pre-coordinated to the vanadium center metal, are confirmed. In addition, the binding properties of oxygen-pre-coordinated VOPc and superoxide ions follow the tendency of empty metal center phthalocyanines (Co, Cu, Mn, and Zn), which show various tendencies depending on the d-orbital occupation. In addition, even in the case of oxygen-pre-coordinated VOPc in which oxygen is already coordinated to the center metal, superoxide ions can bind to the center metal, which means that oxygen-pre-coordinated VOPc can promote the reaction of transferring oxygen to the oxygen electrode in Li–O_2 cell. This result is supported by the first-principles calculation results, which show that oxygen-pre-coordinated VOPc has the most stable energy when the superoxide ion binds to the center metal. In this case, it is preferred to bind the superoxide to the opposite side of the site where the oxygen is pre-coordinated. Moreover, the improved reversibility of the discharge product was confirmed by the *ex situ* characterization results fabricated using oxygen-pre-coordinated VOPc. This study presents the applicability of a new material, 'oxygen pre-coordinated metal phthalocyanine', which can improve the cell performance of Li–O_2 cells, and confirms its potential as an appropriate catalyst that can enhance the cycle performance and reversibility by suppressing side reactions during redox reactions.

Data availability

The data supporting this article have been included as part of the ESI.†

Conflicts of interest

There are no conflicts to declare.

Acknowledgements

This study was supported by the National Research Foundation of Korea (NRF) grant funded by the Korean Government (MSIT) (No. RS-2023-00208983). This work was supported by the Technology Innovation Program (or Industrial Strategic Technology Development Program) (RS-2024-00409900),

(Polyolefine-based ceramic coated separator for sodium battery) funded By the Ministry of Trade Industry & Energy (MOTIE, Korea).

References

1 P. G. Bruce, S. A. Freunberger, L. J. Hardwick and J.-M. Tarascon, *Nat. Mater.*, 2012, **11**, 19–29.
2 S. Ding, X. Yu, Z. F. Ma and X. Yuan, *J. Mater. Chem. A*, 2021, **9**, 8160–8194.
3 W. J. Kwak, N. Rosy, D. Sharon, C. Xia, H. Kim, L. R. Johnson, P. G. Bruce, L. F. Nazar, Y. K. Sun, A. A. Frimer, M. Noked, S. A. Freunberger and D. Aurbach, *Chem. Rev.*, 2020, **120**, 6626–6683.
4 J. Lu, Y. J. Lee, X. Luo, K. C. Lau, M. Asadi, H. H. Wang, S. Brombosz, J. Wen, D. Zhai, Z. Chen, D. J. Miller, Y. S. Jeong, J. B. Park, Z. Z. Fang, B. Kumar, A. Salehi-Khojin, Y. K. Sun, L. A. Curtiss and K. Amine, *Nature*, 2016, **529**, 377–382.
5 D. U. Lee, P. Xu, Z. P. Cano, A. G. Kashkooli, M. G. Park and Z. Chen, *J. Mater. Chem. A*, 2016, **4**, 7107–7134.
6 T. Zhang and H. Zhou, *Angew. Chem., Int. Ed.*, 2012, **51**, 11062–11067.
7 W.-H. Ryu, T.-H. Yoon, S. H. Song, S. Jeon, Y.-J. Park and I.-D. Kim, *Nano Lett.*, 2013, **13**, 4190–4197.
8 J.-H. Kang, J. Lee, J.-W. Jung, J. Park, T. Jang, H.-S. Kim, J.-S. Nam, H. Lim, K. R. Yoon, W.-H. Ryu, I.-D. Kim and H. R. Byon, *ACS Nano*, 2020, **14**, 14549–14578.
9 I. Landa-Medrano, I. Lozano, N. Ortiz-Vitoriano, I. Ruiz de Larramendi and T. Rojo, *J. Mater. Chem. A*, 2019, **7**, 8746–8764.
10 J. B. Park, S. H. Lee, H. G. Jung, D. Aurbach and Y. K. Sun, *Adv. Mater.*, 2018, **30**, 1–13.
11 Y. Ko, H. Park, B. Kim, J. S. Kim and K. Kang, *Trends Chem.*, 2019, **1**, 349–360.
12 I. Kruusenberg, L. Matisen, Q. Shah, A. M. Kannan and K. Tammeveski, *Int. J. Hydrogen Energy*, 2012, **37**, 4406–4412.
13 J. Ma, Y. Liu, P. Zhang and J. Wang, *Electrochem. Commun.*, 2008, **10**, 100–102.
14 M. Lefèvre, E. Proietti, F. Jaouen and J. P. Dodelet, *Science*, 2009, **324**, 71–74.
15 W. Orellana, *Chem. Phys. Lett.*, 2012, **541**, 81–84.
16 W. J. Kwak, A. Mahammed, H. Kim, T. T. Nguyen, Z. Gross, D. Aurbach and Y. K. Sun, *Mater. Horiz.*, 2020, **7**, 214–222.
17 K. P. C. Yao, J. T. Frith, S. Y. Sayed, F. Bardé, J. R. Owen, Y. Shao-Horn and N. Garcia-Araez, *J. Phys. Chem. C*, 2016, **120**, 16290–16297.
18 S. Matsuda, S. Mori, K. Hashimoto and S. Nakanishi, *J. Phys. Chem. C*, 2014, **118**, 28435–28439.
19 S. Matsuda, S. Mori, Y. Kubo, K. Uosaki, K. Hashimoto and S. Nakanishi, *Chem. Phys. Lett.*, 2015, **620**, 78–81.
20 D. Sun, Y. Shen, W. Zhang, L. Yu, Z. Yi, W. Yin, D. Wang, Y. Huang, J. Wang, D. Wang and J. B. Goodenough, *J. Am. Chem. Soc.*, 2014, **136**, 8941–8946.
21 H. S. Kim, B. Kim, H. Park, J. Kim and W. H. Ryu, *Adv. Energy Mater.*, 2022, **12**, 1–10.
22 F. A. Hamprecht, A. J. Cohen, D. J. Tozer and N. C. Handy, *J. Chem. Phys.*, 1998, **109**, 6264–6271.
23 B. Klaumünzer, D. Kröner and P. Saalfrank, *J. Phys. Chem. B*, 2010, **114**, 10826–10834.
24 H. Wang, X. Wang, M. Li, L. Zheng, D. Guan, X. Huang, J. Xu and J. Yu, *Adv. Mater.*, 2020, **32**, 1–21.
25 C. Lee, W. Yang and R. G. Parr, *Phys. Rev. B:Condens. Matter Mater. Phys.*, 1988, **37**, 785–789.
26 A. Schäfer, C. Huber and R. Ahlrichs, *J. Chem. Phys.*, 1994, **100**, 5829–5835.
27 P. J. Stephen, F. J. Devlin, C. F. Chabalowski and M. J. Frisch, *J. Phys. Chem.*, 1994, **98**, 11623–11627.
28 A. Schäfer, H. Horn and R. Ahlrichs, *J. Chem. Phys.*, 1992, **97**, 2571–2577.
29 M. D. Hanwell, D. E. Curtis, D. C. Lonie, T. Vandermeersch, E. Zurek and G. R. Hutchison, *J. Cheminform.*, 2012, **4**, 17.
30 W. H. Ryu, F. S. Gittleson, J. M. Thomsen, J. Li, M. J. Schwab, G. W. Brudvig and A. D. Taylor, *Nat. Commun.*, 2016, **7**, 12925.
31 S. Mandal, R. N. Samajdar, S. Parida, S. Mishra and A. J. Bhattacharyya, *ACS Appl. Mater. Interfaces*, 2022, **14**, 26714–26723.
32 Y. C. Lu and Y. Shao-Horn, *J. Phys. Chem. Lett.*, 2013, **4**, 93–99.
33 Y. Wang and Y. C. Lu, *Energy Storage Mater.*, 2020, **28**, 235–246.
34 H. W. Lee, H. Kim, H. G. Jung, Y. K. Sun and W. J. Kwak, *Adv. Funct. Mater.*, 2021, **31**, 1–11.
35 H. S. Kim, B. Kim, H. D. Lim and W. H. Ryu, *ACS Sustain. Chem. Eng.*, 2022, **10**, 4198–4205.
36 Y. Wang, N. C. Lai, Y. R. Lu, Y. Zhou, C. L. Dong and Y. C. Lu, *Joule*, 2018, **2**, 2364–2380.